The Major Role of London Dispersion Interaction in the Assembly of Cellulose, Chitin, and Chitosan

Yiwei Li, Chunxia Yan, Yu Chen, Xuhui Han, Ziqiang Shao, Haisong Qi, Xiaodong Li, Yoshiharu Nishiyama, Tao Hu, Pan Chen

The Major Role of London Dispersion Interaction in the Assembly of Cellulose, Chitin, and Chitosan

Yiwei Li[1,‡], Chunxia Yan[1,‡], Yu Chen[1], Xuhui Han[1], Ziqiang Shao[1], Haisong Qi[2,*], Xiaodong Li[1], Yoshiharu Nishiyama[3,*], Tao Hu[4,*], Pan Chen[1,*]

[1]*School of Materials Science and Engineering, Beijing Institute of Technology, 100081, Beijing, China*

[2]*State Key Laboratory of Pulp and Paper Engineering, South China University of Technology, Guangzhou 510640, China*

[3]*Université Grenoble Alpes, CNRS, CERMAV, 38000 Grenoble, France*

[4]*School of Materials Science and Engineering, State Key Laboratory of Advanced Special Steels, Shanghai University, Shanghai 200444, China*

Contributed equally.

Corresponding authors: qihs@suct.edu.cn; yoshi@cermav.cnrs.fr; taohu@shu.edu.cn; panchen@bit.edu.cn

Abstract:

Noncovalent interactions are vitally important to understand the structural stability and molecular assembly of cellulose and its analogue molecules. Using density functional theory in conjunction with three popular generations of dispersion correction (D2, D3, D4), we systematically estimate the strength of inter-chain interaction for several β-1,4-linked crystalline polysaccharides (cellulose Iα, Iβ, II, III_I, α-chitin, β-chitin, chitosan) and their building block monomers (glucose, cellobiose). Switching on and off dispersion correction for both condensed and isolated chains allow the extraction of the intra- and inter-chain London dispersion interactions as well as the inter-chain electrostatic interaction. Regardless of the generations of dispersion correction and allomorphs, the estimated inter-chain London dispersion interaction is 45~74 kJ/mol per pyranose ring comparable to the inter-chain electrostatic interaction (47~88 kJ/mol). The upper limit of the strength of inter- or intra-chain hydrogen bonds are estimated to be 21~53 kJ/mol based on energy profiles of hydroxyl rotation. Our work quantitatively highlights that it is the London dispersion interaction rather than the hydrogen bonding interaction dominating in the tight assembly of polymer chains for β-1,4-linked crystalline polysaccharides, regardless of the crystal allomorph and types as well as the generations of dispersion correction of DFT. thus, London dispersion interaction should be preferentially considered during their deconstruction, defibrillation, or dissolution processes.

Introduction:

X-ray and neutron studies revealed abundant hydrogen bonds and regular network patterns among the crystal structures of cellulose and chitin (Langan et al. 1999; Nishiyama et al. 2002; Nishiyama et al. 2003; Wada et al. 2004; Deringer et al. 2016; Ogawa et al. 2019; Sikorski et al. 2009; Nishiyama et al. 2011; Naito et al. 2016). Some authors regarded hydrogen bonds as the key factor governing the assembly of polymer chains, trying to explain many physical properties of cellulose. Recent studies have gradually reshaped such a view. The impact of hydrogen bond on the peeling-off of the cellotetrose (Bergenstråhle et al. 2010) and the proposal of the hydrophobicity of cellulose (Lindman et al. 2010; Lindman et al. 2021; Medronho et al. 2014; Glasser et al. 2012) also argued that the contribution of hydrogen bonding to the insolubility of cellulose was overemphasized.

After a few years of debates, it seems that we have well established hitherto that other noncovalent interactions, such as electrostatic interaction and London dispersion interactions, are also responsible for the tight chain stacking (Jarvis 2023). A more recent, detailed review evaluated the "exaggerated" role of hydrogen bonds (Wohlert et al. 2023) associated with the properties of cellulose in the paste decades. Based on the linear tendencies of heat of evaporation of analogue molecules with number of hydroxyl groups and molecular weights, the inter-chain London dispersion interaction in crystalline cellulose Iβ is estimated to be 67 kJ/mol per glucose while hydrogen bond energy is 24 kJ/mol(Nishiyama 2018). Still, the first-principles-based quantification of internal energy of the cellulose and chitin are rare (Deringer et al. 2016). We previously quantified the partition of the non-covalent interaction in chitin and chitosan based on DFT-D2 calculations (Chen et al. 2021) using energy decomposition analysis base on low-dimensionfragments (Deringer et al. 2016). Here, we have extended this method for the systematical analysis of cellulose, chitin, chitosan, and their allomorphs as well as their monomers using three different generations of dispersion correction approach (D2 (Grimme 2006), D3 (Grimme et al. 2010), D4 (Caldeweyher et al. 2017; Caldeweyher et al. 2019)) in which polarizability was considered. In addition, the upper limit of hydrogen bond strength is estimated based on the energy profile of hydroxyl rotation, providing a basic understanding of the components of noncovalent of the crystalline polysaccharides.

Computational Methods:

Model Construction: Eight types of crystalline polysaccharides, named cellulose Iα (Nishiyama et al. 2003), Iβ (Nishiyama et al. 2002), II (Langan et al. 1999), III_I(Wada et al. 2004), α-chitin-A (Sikorski et al. 2009, Deringer et al. 2016), α-chitin-B (Sikorski et al. 2009, Deringer et al. 2016), β-chitin (Nishiyama et al. 2011), chitosan (Naito et al. 2016)) whose atomic structures are available. β-D-glucose and, β-D--cellobiose (Jeffrey 1968) were also included. The unit cells

and the corresponding fragment of these crystals are all represented in Figure 1. The computational setup is identical to our former study(references), and a detailed description can be found in the following method sections.

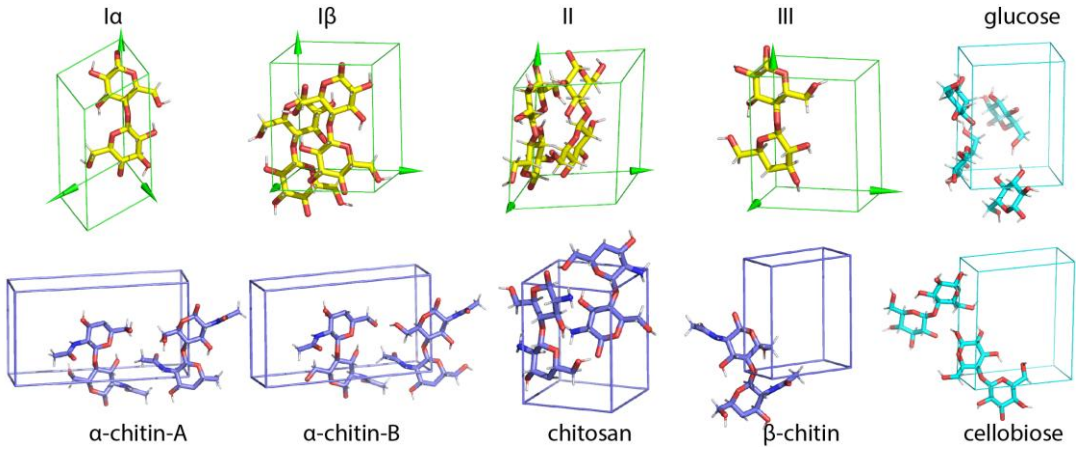

Figure 1. Unit cell representation of cellulose, chitin, chitosan, glucose, and cellobiose. (All crystal structures are deposited in glyco3D)

Energy Minimization: Periodic boundary condition (PBC) based DFT calculation were performed by using Quantum Espresso (QE) (Giannozzi et al. 2009; Giannozzi et al. 2017) and VSAP package. D2 (Grimme 2006) and D3 (Grimme et al. 2010) are implemented in QE and D4 (Caldeweyher et al. 2017; Caldeweyher et al. 2019) can be implemented to VASP (Hafner et al. 1997). The generalized gradient approximation (GGA) functional PBE (Perdew et al. 1996) was used for geometry optimization of crystals. The total energy and force convergence thresholds for ion minimization were set to 1.0e-6 Ry and 1.0e-5Ry/bohr, respectively. The kinetic energy cutoff value of the wave function was 160 Ry. The k-points were set to (2, 2, 2, 0, 0, 0).

Energy Decomposition Analysis: The classical molecular mechanics (MM) represents the intermolecular noncovalent interaction as composed of Coulomb interactions between point charges of each paired atoms and Lennard-Jones potential interactions which includes the London dispersion and Pauli repulsion terms. In DFT calculation, the intermolecular energy is composed of terms such as electrostatics, exchange, induction and dispersion interaction etc. For both cases, we can simplify as dispersion energy and everything else as electrostatic interactions, the molecular interaction energy within a crystal can be written as equation 1.

$$E_{int} = E_{elec} + E_{disp} \quad (1)$$

Further decomposition for intra-chain and inter-chain terms results in four energy terms, which is the interchain electrostatic energy (E_{inter_E}), the intrachain electrostatic energy (E_{intra_E}),

the interchain dispersion energy (E_{inter_D}), and the intrachain dispersion energy (E_{intra_D}) as represented by equation 2.

$$E_{int} = E_{inter\_E} + E_{intra\_E} + E_{inter\_D} + E_{intra\_D} \quad (2)$$

We rely on the low dimensional fragments approach that is widely used in DFT-based materials simulations (Deringer et al. 2016) to estimate the contribution of interchain interactions. In brief, DFT calculation was performed for the three-dimensional crystals (3D: raw unit cell applied with periodic boundary condition), relaxation of both atomic coordinates and crystal lattices, obtaining an optimized energy and structure (noted as E_{3D_disp}, corresponds to top left in Figure 2). One isolated structural fragment (1D) was constructed by computationally "cleaving" the lattice apart from the above fully relaxed 3D structure. This is achieved by leaving one chain within the supercell and enlarging the transverse lattices by a factor of two, which separates this chain from their periodic boundary images, as shown in (top right of) Figure 2. The total-energy computation was subsequently performed by freezing both the box size and coordinates, and the obtained energy is noted as E_{1D_disp}. This is slightly different from our previous work (Chen et al. 2022), in which the enlarged box and atoms were both relaxed, and makes the E_{intra_E} truly constant, In the previous studies the E_{intra_E} was "assumed" to be unchanged which turned out to be not the case as can be seen in the comparison between Table 1 and Table S1. By switching off the dispersion correction and freezing the atoms in the 3D system when dispersion correction switched off and in 1D system when dispersion correction was turned on and off, two other energy terms can be generated, noted as E_{3D_nodisp} and E_{1D_nodisp}, corresponding to the bottom left and right states in Figure 2, respectively. This is illustrated in equation 3, 4, and 5, respectively.

$$E_{intraD} = (E_{1D\_disp} - E_{1D\_nodisp})/N \quad (3)$$

$$E_{inter\_D} = (E_{3D\_disp} - E_{3D\_nodisp})/N - E_{intra\_D} \quad (4)$$

$$E_{inter\_E} = E_{3D\_nodisp}/N \quad (5)$$

Where N stands for the number of residue per unit cell.

The cohesion energy of crystals per residue equals to the sum of E_{inter_D} and E_{inter_E} (equation 6).

$$E_{cohe\_E} = E_{inter\_D} + E_{inter\_E} \quad (6)$$

The graphical illustration of such energy decomposition with cellulose Iβ as a trial is shown in Figure 2. On the graph, E_{1D_disp} is total energy of one isolated structural fragment with dispersion correction switched on. In contrast, E_{1D_nodisp} is the one without dispersion correction.

For E_{3D_disp} and E_{3D_nodisp}, the 3D subscript means a standard unit cell with periodic boundary condition applied and thus the crystal is three dimensional infinite. Disp. and Nodisp indicated whether or not the dispersion correction is applied.

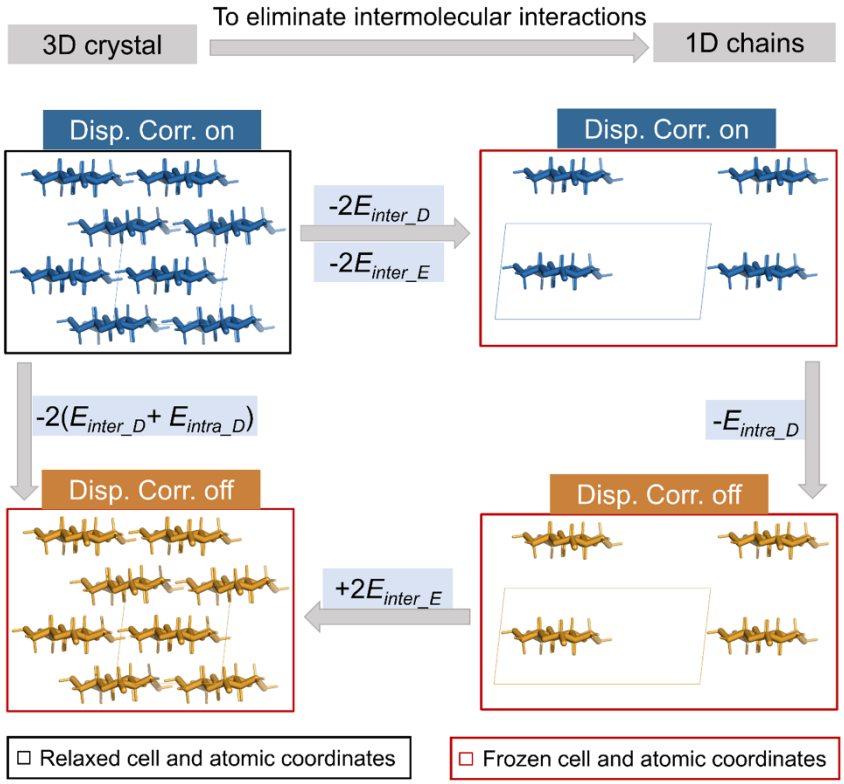

Figure 2. Illustration of the condensed 3D fragment and isolated 1D fragment with dispersion correction switched on/off used for the energy composition calculation.

Table 1. Decomposed energy (E_{inter_E}, E_{inter_D}, E_{intra_D}, E_{Cohe_E}) of crystals.

Energy (-kJ/mol)		Glu	CB	Iα	Iβ	II	III_I	α-chitin-A	α-chitin-B	β-chitin	Chitosan
D2	Intra_D	59	68	70	79	77	76	105	104	105	83
	Inter_D	98	79	62	62	64	60	70	74	70	67
	Inter_E	145	107	50	47	70	63	68	56	72	48
	Cohe_E	243	186	111	109	134	123	139	130	141	116
D3	Intra_D	38	44	52	52	51	51	70	69	70	54
	Inter_D	83	66	53	53	54	48	60	63	59	59
	Inter_E	148	111	54	51	70	69	72	60	76	49
	Cohe_E	231	177	107	105	124	117	132	124	136	108
D4	Intra_D	62	69	78	79	76	77	104	104	104	82
	Inter_D	76	61	48	49	51	45	55	58	56	51
	Inter_E	151	117	61	52	75	69	73	61	88	52
	Cohe_E	227	178	109	100	126	114	128	119	144	103

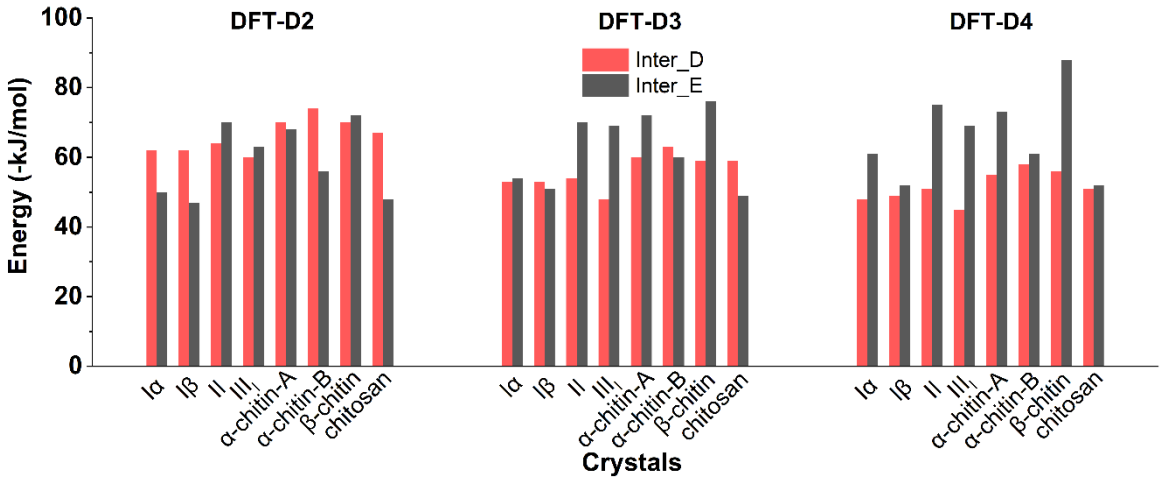

Figure 3. Histogram of intermolecular London dispersion and electrostatic energies (the two components of $E_{\text{Cohe\_E}}$) based on DFT-D2 (left), D3(middle), and D4(right).

Results and Discussion:

Estimation of London Dispersion Interaction

Figure 3 and Table 1 show the decomposed energy for all crystals as a function of generation types of dispersion correction. The (E_{intra_D}, E_{inter_D}, E_{inter_E}, $E_{Cohe.\_E}$) of Iβ is estimated as (79, 62, 47, 109) kJ/mol per glucose based on DFT-D2, respectively. This quantification of E_{inter_D} is close to the empirical estimation of 67 kJ/mol (Nishiyama 2018). Comparing the four allomorphs of cellulose within D2 framework, the E_{inter_D} of II is the largest (64 kJ/mol per glucose), while that of III_I is the smallest (60 kJ/mol per glucose), and Iα/Iβ is in the middle (62 kJ/mol per glucose). If we simply normalize the energy by the volume of their unit cell and considering the relative volume of Iβ being as 1, we obtained xxx for cellulose and xxx for chitin, respectively. Overall, the estimated E_{inter_D} for all polysaccharide crystals ranges from 60 to 74 kJ/mol per glucose, the E_{intra_D} vary from 76 to 105 kJ/mol per glucose, and the E_{inter_E} vary from 47 to 70 kJ/mol based on DFT-D2 calculation. In fact, one can find (Table 1) in crystalline monomer and dimer that the E_{intra_D} (59, 68 kJ/mol) and E_{inter_D} (98, 79 kJ/mol) are (although different but) already comparable to that of polymer crystals. The slightly higher value of E_{inter_D} and smaller value of E_{intra_D} in small molecular crystal than polymer crystal is simply ascribed to the increased molecular weight of repeat unit (162 for anhydrous glucose, 171 for cellobiose, and 180 for glucose). Different hydroxy groups per glucose also leads to different number of inter-molecular hydrogen bonds per residue, which is 5 for glucose, 4 for cellobiose and 2 for II, III_I, chitin, and 1 for Iα/Iβ and chitosan. Because the component nature of

hydrogen bonds is mostly electrostatic interaction, the E_{inter_E} in small molecular crystals is both much larger than its E_{inter_D} (Figure S1) and E_{inter_E} of polymer crystals, respectively. For a quick and rough calculation, we simply divide the E_{inter_E} by the number of hydrogen bonds per residue, the strength of the single hydrogen bond in mono and dimer crystals can be estimated to be under 30 kJ/mol in glucose and 27 kJ/mol in cellobiose. Similarly, the E_{inter_E} in cellulose II, III_I, and chitin are larger than Iα, Iβ, and chitosan, simply due to one more inter-chain hydrogen bond per glucose residue. More measurement of hydrogen bonds interaction will be discussed in the last section.

Based on the DFT-D2 calculation, for the β-1,4-linked crystalline polysaccharides, the London dispersion interaction represents by 48~58% of the total cohesion energy of the polymer crystal regardless of polymer categories and types of correction used as can be overviewed in Figure 3 (left) and Table 3.

The Impact of Three Generations of Dispersion Correction

When dispersion correction was modulated from D2 to the other two generations (D3 and D4), the four energy terms (E_{intra_D}, E_{inter_D}, E_{inter_E}, $E_{Cohe.\_E}$) of cellulose Iβ varied to (52, 53, 51, 105 kJ/mol) for D3 and (79, 49, 52, 100 kJ/mol) for D4, showing the monoclinic decreasing of E_{inter_D} and the increase of E_{inter_E} and resulting the E_{inter_E} slightly over E_{inter_D}. Such tend of reverse between E_{inter_D} and E_{inter_E} is also applicable for other crystals as presented in Figure Sxx. In D2, the dispersion coefficients for each atom species were constant no matter their chemical contexts. In D3 and D4, the local electron polarizability effect was accounted for and the dispersion coefficients are automatically adjusted according to their local chemical environment, resulting in more expensive calculations and different energy values. Such update leads to slightly difference in predicted unit cell parameters, especially the slightly expansion of unit cell parameter a, which reflected the relatively less tight packing in D3 and D4, and therefore reduced E_{inter_D} and increased E_{inter_E}. Still, the E_{inter_D} takes 41~55% of the total intermolecular interactions for D3, and 35~48% for D4, as shown in Table S7.

No matter which type of dispersion correction, the E_{inter_D} and E_{intra_D} of chitin is always higher than cellulose. This is simply ascribed to the larger molecular weight of the repeat unit (which is 162 Da for cellulose, and 203 Da for chitin).

Estimations of hydrogen bond strength

Although more than one hundred years have passed since the first proposal for hydrogen bond (Huggins1971; Derewenda et al. 2021), the estimation of its range of the strength is still under development (Emamian et al. 2019). To computationally estimate one hydrogen bond interaction between small molecules such as water, one can simply separate the hydrogen bonding paired molecules and estimated the energy difference as hydrogen bond strength since the London dispersion interaction is small and thus can be neglected. However, for hydrogen bonds in cellulose or chitin, one cannot simply do so because of other electrostatic interactions and the increased London dispersion due to increased molecular weight. In addition, dividing the E_{inter_E} by the number of interchain hydrogen bonds would overestimate the hydrogen bond contribution, because other multipolar electrostatic interactions also contribute to E_{inter_E}. In the textbook (Mark 2023), an hydrogen bonds are often judged by an arbitrary geometric factors: donor (H)-acceptor length < 0.27 nm and H-donor-acceptor angle < 30°. When such criteria are not fulfilled, they fall into categories of Coulomb interaction. Based on this, we developed an approach by extracting one chain or one sheet out of the 3D crystal (as shown in Figure 4) and rotating the hydroxyl group around the C-O bond. Single point energy calculations were run at each point by freezing all the atoms. Only a proton is moving so the London dispersion interaction can be regarded as nearly constant and the energy difference can be regarded as an indicator of hydrogen bond and partial contribution from electrostatic repulsion interaction. This method is similar to the study by Estácio et al (Estácio et al. 2004) which shows that this hydrogen bond energy value is overestimated and can be considered as an upper limit of hydrogen bond strength. Details for each hydrogen bond energies in β-chitin are also provided in Figure S2.

Taking the intrachain hydrogen bond of Iβ as an example, the HO3-O3 was rotated around the O3-C3 bond with a stepwise increment of 10° starting from the initial energy minimum (labeled as A) and single point energy was calculated at each frame, as shown in Figure 4. The variation of total energy is purely ascribed to the movement of hydrogen (HO3) atom. The difference between the optimized energy and when H-O…H angle becomes 30° is considered as the strength of intra-chain O3H…O5 hydrogen bond (labeled as B in the Figure 4a). The estimation of another intra-chain (O2-HO2…HO6) hydrogen bond was done in a similar way by applying rotation for O2-HO2 around the C2-O2 bond as shown in Figure 4b. The estimation of inter-chain hydrogen bond (O6-HO6...O3) requires the simultaneous rotations of C2-O2-HO2 and C6-O6-HO6 angles, because the sole rotation of C6-O6-HO6 will induce short HO6…HO2 contact (< 1 Å) that is unreasonable. To avoid this short proton-proton contact, starting from the energy minima, the HO2 hydroxyl and HO6 hydroxyls are rotated in an

opposite direction as indicated in the red arrow in Figure 4c. The rotation of HO2 in Figure 4c and 4b follows the same direction. The total energy variation of simultaneous rotation of HO2 and HO6 was subtracted by the energy profiles of the sole HO2 rotation in Figure 4b, and the result in shown in Figure 4c. The estimation of other crystals follows the receipt of Iβ.

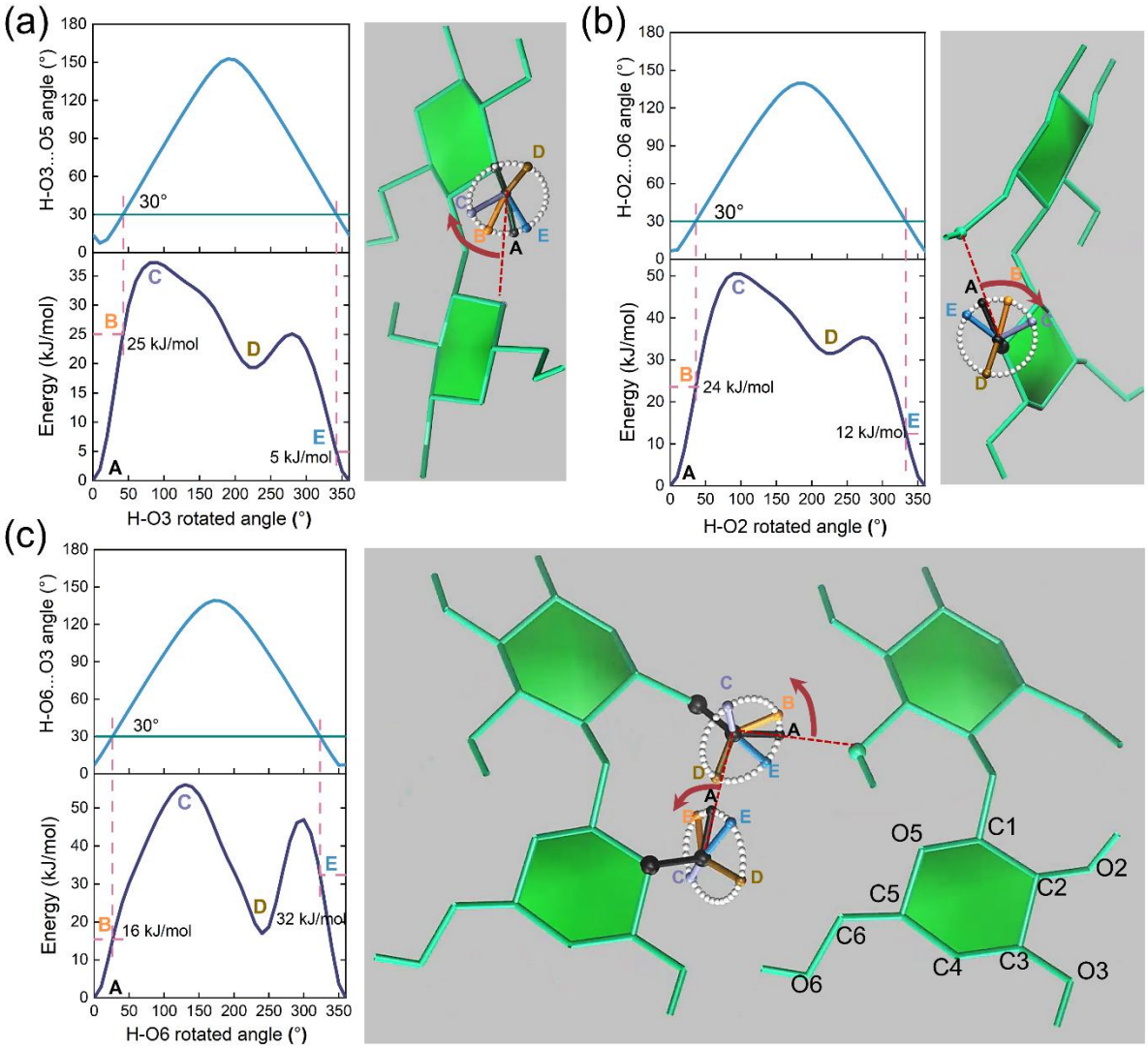

Figure 4. Total energy variation of Iβ chain as the function of H-O rotated angle around bond C-O. The arrow indicates the rotation trajectory of hydroxyl groups. A, B, C, D, E in energy profiles corresponds to the same label in molecular snapshots which indicates the selected frames during the rotation trajectory of hydroxyls. The red arrows indicate the rotational direction of hydroxyls from 0 to 360 degree.

By setting the universal hydrogen bond criteria (H…acceptor < 0.27 nm and H-D-A < 30°), the three major hydrogen bond ($E_{HO3...O5}$, $E_{HO2...O6}$, $E_{HO6...O23}$) of Iβ can be qualitatively estimated to have the upper limit of 25 kJ/mol, 24 kJ/mol, and 31 kJ/mol, with DFT-D2 as labeled in the dashed line in Figure 4a, 4b, and 4c. The slightly higher value of $E_{HO6...O3}$ than the

other two can be ascribed to the additional contribution of electrostatic attraction from the HO6…O2 pair, since the rupture of HO6…O3 also alters the HO6…O2 distance during the rotation of hydroxyl group (Figure 4 & S3). Summary of all hydrogen bond strength is provided in Table 2, showing the range from 14 to 33 kJ/mol, which is similar to that in the estimation of alcohol hydrogen bond (24 kJ/mol) of small analogs (Nishiyama 2018). This indicates that the hydrogen bond strength in cellulose, chitin, and chitosan is not particularly strong, but is similar to their smaller analogs (such as glucose, Table S2). For the chitin and chitosan, the strength of NH…OC hydrogen bond is 26 or 34 kJ/mol, within the same magnitude of the strength of OH…OH hydrogen bond of cellulose. All the hydrogen bond strength estimation depends very little on the generation types of London dispersion correction, as shown in Table S3, S4 (13~34 kJ/mol for D3) and S5 (14~32 kJ/mol for D4), for all crystals.

Table 2. The type and maximum strength of intra- and inter-chain hydrogen bond (HB) in crystals.

Energy (-kJ/mol)		Iα	Iβ	II	III_I	α-chitin-A	α-chitin-B	β-chitin	Chitosan
Intra-HB	O3H…O5	25	26	21	21	27	32	27	27
	O2H…O6	23	24	--	--	--	--	--	--
	O6H…O3	33	31	--	--	--	--	--	--
Inter-HB	O6H…O2	--	--	16	21	--	--	--	--
	O2H…O6	--	--	19	23	--	--	--	--
	O2H…O2	--	--	14	--	--	--	--	--
	O6H…O6	--	--	30	--	--	20	--	--
	O6H…OC	--	--	--	--	13	--	17	--
	NH…OC	--	--	--	--	33	30	33	--
	O6H…N	--	--	--	--	--	--	--	27

Each anhydrous glucose residue in Iβ contains three free hydroxyl groups that form one interchain hydrogen bond and two intra-chain hydrogen bond on average, the strength of which is <31 and <50 kJ/mol per glucose, proving that both the inter- and intra-chain hydrogen bond strengths are less stronger than the corresponding London dispersion interactions (62 and 79 kJ/mol per glucose) respectively. This picture is regardless of types of dispersion correction (52, 51, 53, 27 of E_{intra_D}, E_{intra_HB}, E_{inter_D}, E_{inter_HB} for D3 and 79, 53, 49, 31 for D4). A similar expression also applies to cellulose Iα that exhibits similar structural features as Iβ, as shown in Table 3.

Table 3. Comparison between London dispersion **interaction and hydrogen bond.**

		Iα	Iβ	II	III_I	α-chitin-A	α-chitin-B	β-chitin	Chitosan
D2	Intra_D	79	79	77	76	105	104	105	83
	Intra HB	48	50	21	21	27	32	27	27

	Inter_D	62	62	64	60	70	74	70	67
	Inter HB	33	31	40	44	46	50	50	27
D3	Intra_D	52	52	51	51	70	69	70	54
	Intra HB	49	51	22	29	26	31	26	27
	Inter_D	53	53	54	48	60	63	59	59
	Inter HB	29	27	37	39	47	44	50	27
D4	Intra_D	78	79	76	77	104	104	104	82
	Intra HB	48	53	21	29	26	32	28	27
	Inter_D	48	49	51	45	55	58	56	51
	Inter HB	32	31	39	34	45	44	47	28

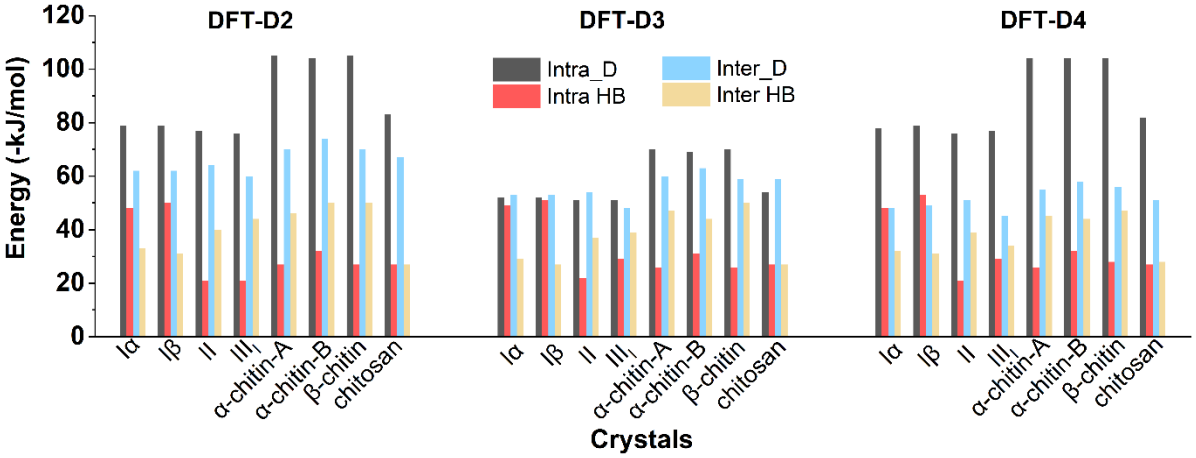

Figure 5. Histogram of (inter-chain and intra-chain) London dispersion interaction and hydrogen bond strength in crystals.

For other cellulose allomorphs (II and III_I) and chitin, as well as chitosan, the intra-chain hydrogen bond (O3H…O5) is retained but the planar hydrogen-bond network disappears due to the conformational variation of the exocyclic hydroxylmethyl group, which is *tg* in native cellulose, *gg*/*gt* in α-chitin, and *gt* in the rest. The number of inter-chain hydrogen bonds increases from 1 to 2 per residue and the intra-chain one decreases from 2 to 1, thus accompanying with the increased total strength of inter-chain hydrogen bonds. However, the strength of inter-chain hydrogen bonds is always below 50 kJ/mol from D2, 50 kJ/mol from D3, and 47 kJ/mol from D4, showing that none of them exceeds their corresponding inter-chain London dispersion interaction (see Table 3). Regarding the intra-chain interactions, hydrogen bonds contribute far less than dispersion interaction (<32 kJ/mol versus >50 kJ/mol, respectively) as also shown in Table 3. The same picture between intra- and inter-chain dispersion interactions and hydrogen bonds also holds for other polysaccharide analogues. As shown in the Table S6, the component of hydrogen bonding interaction in the total interchain interaction in crystals varies between 23%

and 40% while that of London dispersion energy fluctuates between 35% and 58% (Table S7), and the electrostatic interactions overall occupied from 42% to 61% (Table S8).

When hydroxyl groups is rotated around their corresponding CO bond (Figure 4), the energy barrier during the C-O-H angle rotation may reach 50~60 kJ/mol per residue. One may simply think this should be considered as the hydrogen bond strength. Such thought is improper because the energy variation induced by the rotation of hydroxyl group includes both hydrogen bond and other repulsions or attractions between hydrogen and nearby atoms. This repulsion or attraction occurs in polymers but not for small molecules (such as water) in isolated state due to steric effect of adjacent atoms in polymer chain. One obvious evidence is the bimodal shape of the energy profile, where an energy minimum occurs between 200º and 250º, and is due to the electrostatic attraction between mobile hydrogen and its adjacent oxygen. Their geometry parameters at this minimum are far beyond the standard hydrogen bond criteria. At this low energy minimum, the nearby electrostatic repulsion is the most minor and the energy variation is always less than 32 kJ/mol in comparison to the initial state (20 kJ/mol in Figure 4a, 32 kJ/mol in Figure 4b, 18 kJ/mol in Figure 4c), which is much smaller than the energy barrier. Therefore, our estimated energy difference is already the upper limit of hydrogen bond strength.

The fact that hydrogen bond strength estimated here is slightly higher than those reported for small molecules is that one hydroxyl in polysaccharide crystal structures acts as both donor and acceptor because of the hydrogen bonding network, resulting in constructing correlation among each hydrogen bond. Influencing one may also partially interrupt others. The cooperativity in hydrogen bond network is also reported to enhance the strength of a single hydrogen bond, but the extent is limited (Qian 2008; Masella et al. 2000). The hydrogen bond strength is also reported to be context-dependent in protein, which is stronger in the inner hydrophobic core than surface but never found to dominate the structural stability.(Deechongkit et al. 2004) A similar principle can be parallel to crystalline polysaccharides according to our estimation and London dispersion interaction.

Conclusion:

To summarize, using DFT calculation and modulation of dispersion correction and the single energy calculation with rotating hydroxyl groups, we have systematically quantified the London dispersion interaction and strength of hydrogen bond of cellulose, chitin, and chitosan and their monomer and dimers. We are able to confirm the fact that inter-chain London dispersion interaction excesses the strength of inter-chain hydrogen bond within the lattice energy of cellulose Iβ as Nishiyama reported. In addition, the intra-chain London dispersion

interaction was proved to also be stronger than the intra-chain hydrogen bonds for Iβ crystals. Moreover, these findings not only adapt to cellulose Iβ, but also to other cellulose allomorphs (Iα, II, III_I) and other β-(1,4)-crystalline polysaccharides (chitin and chitosan). Although the alteration of different generations of dispersion interactions alters slightly the absolute value of intermolecular dispersion and electrostatic as well as hydrogen bonding energies due to slightly different unit cell parameters comparing to experimental observation, the picture that London dispersion interaction excesses hydrogen bonding interaction always stands. Our quantification provides direct evidence that refutes the hydrogen bonding dominated dissolution mechanism of cellulose and chitin. One may argue that although one hydrogen bond is not strong enough, the activation energy of peeling-off abundant hydrogen bonds along a polymer chain would be strong. This is true, but the peeling-off energy required to resist London dispersion interaction in crystal would also be strong, and still larger than the total energy of many hydrogen bonds.

Ethics approval and consent to participate

All authors state that they adhere to the Ethical Responsibilities of Authors. In addition, this article does not contain any studies with human participants or animal performed by any of the authors.

Competing Interests

Not applicable

Availability of data and materials

Not applicable

Competing interests

The authors have no relevant financial or non-financial interests to disclose.

Funding

This research was supported by the Beijing Natural Science Foundation (2232064).

Author Contributions

YL & CY: Investigation, data analysis, original draft. Y C & XH: Investigation. ZS & XL: Resources and review. HQ & Y. Nishiyama & TH: Supervision and review. PC: Project administrator, investigation, supervision, original draft and review. All authors read and approved the final manuscript.

Acknowledgements

PC thanks the Beijing Natural Science Foundation (2232064).

References

Bergenstråhle M, Wohlert J, Himmel M E, Brady J W (2010) Simulation studies of the insolubility of cellulose. Carbohydr. Res 345(14): 2060–2066. https://doi.org/10.1016/j.carres.2010.06.017Caldeweyher E, Bannwarth C, Grimme S (2017) Extension of the D3 dispersion coefficient model. J Chem Phys 147 (3): 034112. https://doi.org/10.1063/1.4993215

Caldeweyher E, Ehlert S, Hansen A, Neugebauer H, Spicher S, Bannwarth C, Grimme S (2019) A generally applicable atomic-charge dependent London dispersion correction. J Chem Phys: 150 (15), 154122. https://doi.org/10.1063/1.5090222

Chen P, Nishiyama Y, Putaux J-L, Mazeau K (2014) Diversity of potential hydrogen bonds in cellulose I revealed by molecular dynamics simulation. Cellulose 21 (2): 897-908. https://doi.org/10.1007/s10570-013-0053-x

Chen P, Nishiyama Y, Wohlert J (2021) Quantifying the influence of dispersion interactions on the elastic properties of crystalline cellulose. Cellulose 28 (17): 10777-10786. https://doi.org/10.1007/s10570-021-04210-0

Chen P, Ogawa Y, Nishiyama Y, Bergenstråhle-Wohlert M, Mazeau K (2015) Alternative hydrogen bond models of cellulose II and III_I based on molecular force-fields and density functional theory. Cellulose 22 (3), 1485-1493. https://doi.org/10.1007/s10570-015-0589-z

Chen P, Zhao C J, Wang H Y, et al. (2022) Quantifying the Contribution of the Dispersion Interaction and Hydrogen Bonding to the Anisotropic Elastic Properties of Chitin and Chitosan[J]. Biomacromolecules 23(4): 1633–1642. https://doi.org/10.1021/acs.biomac.1c01488

Deechongkit S, Nguyen H, Powers E, et al. (2004) Context-dependent contributions of backbone hydrogen bonding to β-sheet folding energetics. Nature 430: 101–105. https://doi.org/10.1038/nature02611

Derewenda Z S (2021) On the centennials of the discoveries of the hydrogen bond and the structure of the water molecule: the short life and work of Eustace Jean Cuy (1897–1925). Acta Crystallogr., Sect. A. https://doi.org/10.1107/S205327332100

Deringer V L, Englert U, Dronskowski R (2016) Nature, strength, and cooperativity of the hydrogen-bonding network in α-chitin. Biomacromolecules 17 (3): 996-1003. https://doi.org/10.1021/acs.biomac.5b01653

Emamian S, Lu T, Kruse H, Emamian H (2019) Exploring Nature and Predicting Strength of Hydrogen Bonds: A Correlation Analysis Between Atoms-in-Molecules Descriptors, Binding Energies, and Energy Components of Symmetry-Adapted Perturbation Theory. J. Comput. Chem 40: 2868-2881. https://doi.org/10.1002/jcc.26068

Estácio S G, Cabral do Couto P, Costa Cabral B J, et al. (2004). Energetics of Intramolecular Hydrogen Bonding in Di-substituted Benzenes by the ortho-para Method. J. Phys. Chem. A 108(49), 10834-10843. https://doi.org/10.1021/jp0473422

Glasser W G, Atalla R H, Blackwell J, Malcolm B R, et al. (2012) About the structure of cellulose: debating the Lindman hypothesis. Cellulose 19 (3): 589-598. https://doi.org/10.1007/s10570-012-9691-7

Grimme S (2006) Semiempirical GGA-type density functional constructed with a long-range dispersion correction. J Comput Chem 27 (15), 1787-99. https://doi.org/10.1002/jcc.20495

Grimme S, Antony J, Ehrlich S, Krieg H (2010) A consistent and accurate ab initio parametrization of density functional dispersion correction (DFT-D) for the 94 elements H-Pu. J Chem Phys 132 (15): 154104. https://doi.org/10.1063/1.3382344

Huggins M L (1971) 50 Years of Hydrogen Bond Theory. Angew. Chem., Int. Ed. Engl.10(3):147-152. https://doi.org/10.1002/anie.197101471

Jarvis M C (2023) Hydrogen bonding and other non-covalent interactions at the surfaces of cellulose microfibrils. Cellulose 30: 667-687. https://doi.org/10.1007/s10570-022-04954-3

Jeffrey G (1968) The refinement of the crystal structures of β-D-glucose and cellobiose. Acta Crystallogr., Sect. B: Structural Crystallography and Crystal Chemistry 1968, 24 (6), 830-838. https://doi.org/10.1107/S0567740868003250

Langan P, Nishiyama Y, Chanzy H (1999) A revised structure and hydrogen-bonding system in cellulose II from a neutron fiber diffraction analysis. J. Am. Chem. Soc 121 (43): 9940-9946. https://doi.org/10.1021/ja9916254

Lindman B, Karlström G, Stigsson L (2010) On the mechanism of dissolution of cellulose. Journal of molecular liquids 156 (1): 76-81. https://doi.org/10.1016/J.MOLLIQ.2010.04.016

Lindman B, Medronho B, Alves L Norgren M, Nordenskiöld L (2021) Hydrophobic interactions control the self-assembly of DNA and cellulose. Q. Rev. Biophys 54: 33541444. https://doi.org/10.1017/S0033583521000019

Mark A, Andrey A, Cathrine B, et al. (2023) GROMACS 2023 Manual (Version 2023). Zenodo. https://doi.org/10.5281/zenodo.7588711

Masella M, Flament J P (2000) Influence of cooperativity on hydrogen bond networks. Mol Simul 24(1-3): 131-156. https://doi.org/10.1080/08927020008024192

Medronho B, Lindman B (2014) Competing forces during cellulose dissolution: from solvents to mechanisms. Curr Opin Colloid Interface Sci 19 (1): 32-40. https://doi.org/10.1016/j.cocis.2013.12.001

Naito P K, Ogawa Y, Sawada D, Nishiyama Y, Iwata T, Wada M (2016) X- ray crystal structure of anhydrous chitosan at atomic resolution. Biopolymers 105 (7), 361-368. https://doi.org/10.1002/bip.22818

Nishiyama Y (2018) Molecular interactions in nanocellulose assembly. Philos. Trans. Royal Soc. A 376 (2112): 20170047. https://doi.org/10.1098/rsta.2017.0047

Nishiyama Y, Langan P, Chanzy H (2002) Crystal structure and hydrogen-bonding system in cellulose Iβ from synchrotron X-ray and neutron fiber diffraction. J. Am. Chem. Soc 124 (31): 9074-9082. https://doi.org/10.1021/ja0257319

Nishiyama Y, Noishiki Y, Wada M (2011) X-ray structure of anhydrous β-chitin at 1 Å resolution. Macromolecules 44 (4): 950-957. https://doi.org/10.1021/ma102240r

Nishiyama Y, Sugiyama J, Chanzy H, Langan P (2003) Crystal structure and hydrogen bonding system in cellulose Iα from synchrotron X-ray and neutron fiber diffraction. J. Am. Chem. Soc 125 (47): 14300-14306. https://doi.org/10.1021/ja0257319

Ogawa Y, Naito P -K, Nishiyama Y (2019) Hydrogen-bonding network in anhydrous chitosan from neutron crystallography and periodic density functional theory calculations. Carbohydr. Polym 207: 211–217. https://doi.org/10.1016/j.carbpol.2018.11.042

Qian X (2008) The effect of cooperativity on hydrogen bonding interactions in native cellulose Iβ from ab initio molecular dynamics simulations, Mol Simul, 34 (2): 183-191. https://doi.org/10.1080/08927020801961476

Sikorski P, Hori R, Wada M (2009) Revisit of alpha-chitin crystal structure using high resolution X-ray diffraction data. Biomacromolecules10 (5): 1100-1105. https://doi.org/10.1021/bm801251e

Wada M, Chanzy H, Nishiyama Y (2004) Cellulose III$_I$ Crystal Structure and Hydrogen Bonding by Synchrotron X-ray and Neutron Fiber Diffraction. Macromolecules 37 (23): 8548-8555. https://doi.org/10.1021/ma0485585

Wohlert M, Benselfelt T, Wågberg L, Furó I, Berglund L A, Wohlert J (2023) Cellulose and the role of hydrogen bonds: not in charge of everything. Cellulose 29 (1): 1-23. https://doi.org/10.1007/s10570-021-04325-4